PCCP

Accepted Manuscript

ROYAL SOCIETY OF CHEMISTRY

www.rsc.org/pccp

Physical Chemistry Chemical Physics
CREATED USING THE RSC LaTeX PCCP ARTICLE TEMPLATE – SEE www.rsc.org/electronicfiles FOR DETAILS
ARTICLE TYPE www. rsc.org/xxxxxx | XXXXXXXX

Sorting particles with nanoscale thermophoretic devices: how efficient is it?†

Anders Lervik[*a] **and Fernando Bresme**[*b]

Received Xth XXXXXXXXXX 20XX, Accepted Xth XXXXXXXXX 20XX
First published on the web Xth XXXXXXXXXX 200X
DOI: 10.1039/b000000x

We investigate particle separation driven by thermal gradients across solid state nanopores using a combined molecular dynamics simulation, non-equilibrium thermodynamics theory and a kinetic model approach. The thermophoretic device, a thermal nanopump, exploits thermal gradients to sort particles of different mass, which accumulate preferentially in hot or cold reservoirs. We show that the large amount of energy dissipated by the thermal nanopump during the transport process leads in general to very low efficiencies, 0.01-0.15%. We find that the nanopump thermal conductivity and structure plays a crucial role in determining the efficiency and a route to enhance it. Doubling the pore radius, from 0.5 - 1 nm radius, leads to a large increase in the mass diffusion and to a 20 fold increase in the efficiency. Addition of nanoscale defects, without modification of the nanopore structure, leads to a large reduction of the nanopump thermal conductivity and to a large enhancement of the thermodynamic efficiency. We find that nanopumps with nanoscale defects are > 3 times more efficient than those without defects. Finally, we identify the microscopic variables responsible for the enhancement of thermally induced transport across nanopores and discuss strategies to tune these variable in order to regulate transport efficiency.

1 Introduction

A significant amount of the energy employed in human activities is dissipated as heat. Recent estimates indicate that the dissipated heat amounts to over half of the energy consumed worldwide[1]. There is considerable interest in the investigation of physical principles that can be used to recover this large amount of wasted heat and convert it into other useful forms of energy. The thermal gradients resulting from heat dissipation processes can induce an interesting and useful range of physical phenomena: thermodiffusion, thermophoresis (the Soret effect) and thermoelectricity are well known coupling effects[2]. More recent studies have also shown the possibility of manipulating the rotational degrees of freedom of molecular structures so that the molecules adopt preferred orientations. Non-equilibrium thermodynamics theory has been employed to rationalize this phenomenon and a link with thermodiffusion has been established[3,4]. Thermal gradients arising from heat dissipation, particularly at small scales (sub micrometer), provide a route to manipulate molecules and particle suspensions and a physical principle to develop nanodevices with potential uses in particle separation and sensors[5–9].

Separation and analytical devices often involve a membrane, *i.e.*, a physical barrier that separates solutions with different compositions. The membrane can be decorated with nanopores, which act as gates for the selective passage of molecules. Nanopores can be manufactured with great precision, making it possibly to develop novel sensor technologies, providing new opportunities in analytical chemistry[10–12]. The use of thermal gradients as driving forces to translocate molecules through nanopores[9,13] or to induce motion in microdevices[14] has also been highlighted. Working at the small scales characteristic of nanomaterials offers some distinctive advantages, as it is possible to generate very large thermal gradients with temperature differences of a few degrees. Because the thermal gradient is the driving force for thermodiffusion, larger gradients should produce more significant effects. Large gradients, in the range 10^{6-9} K/m have been achieved optical trapping experiments of colloids[15] and in experiments thermophoretic motion in nanotubes[16]. These huge gradients should result in strong thermophoretic responses that can be employed to control the kinetics of molecular translocation through nanopores.

The combination of thermophoretic forces and nanopore structures provides an approach to design *thermal nanopumps* with potential applications in mass separation processes. In this article we investigate particle separation in a fluid binary mixture consisting of two reservoirs with the same composition and separated by a solid state nanopore. A thermal gradient across the nanopore provides the driving force for the selective transfer of particles across the reservoirs. We em-

[a] *Department of Chemistry, Imperial College London, SW7 2AZ, London UK; E-mail: anders.lervik07@imperial.ac.uk*
[b] *Department of Chemistry, Imperial College London, SW7 2AZ, London UK; E-mail:f.bresme@imperial.ac.uk*

ploy in this work atomistic non-equilibrium computer simulations to model the separation process. Computer simulations have been successfully employed before to investigate transport across nanopores in osmosis [17], DNA sensing [18] and fluid flow through nanofluidic channels [19]. However most of these works have considered electric and pressure gradients as driving forces to induce particle flow instead of thermal gradients. We combine the computer simulations with non-equilibrium thermodynamics theory [2,20] and kinetic models, in order to establish correlations between the thermodynamic efficiency of the transport process and the structural features of the nanopores.

At the nanoscale, fluctuations play a larger role and the efficiency can feature strong variations. This has been demonstrated in molecular motors, where efficiencies in the range of 10-100 % have been reported [21–25]. There is also evidence that the efficiency of model nanomotors powered by chemical reactions can be extremely low $\sim 0.02\%$ [26]. We will show that the efficiency of thermal nanopumps can also be very low and feature a strong dependence with nanopore structure. Based on our results we identify strategies to enhance the transport efficiency of thermal separation processes.

2 Heat and mass transport across the nanopump

Our *thermal nanopump* exploits the Soret-Ludwig effect to selectively transfer particles between two reservoirs held at different temperatures, $T_{\rm H}$ and $T_{\rm C}$ (see Figure 1). In our investigation the heavy and light particles preferentially migrate to the cold and hot reservoirs respectively. Each reservoir contains a binary mixture of particles A and B that are identical in size, $\sigma_{\rm A}/\sigma_{\rm B} = 1$, but with different masses, such that $m_{\rm A}/m_{\rm B} = 10$. The nanopump is modeled as a crystalline structure of atoms of a third kind of species, labelled NP. The interactions were modeled using the Lennard-Jones potential, $u_{ij}(r) = 4\varepsilon_{ij}\left[(\sigma_{ab}/r)^{12} - (\sigma_{ab}/r)^{6}\right]$ between species i, j, with $\varepsilon_{ij} = \sqrt{\varepsilon_{ii}\varepsilon_{jj}}$ and $\sigma_{ij} = 0.5(\sigma_i + \sigma_j)$. The interactions between the fluid particles, A − A, A − B and B − B, and between fluid and nanopump particles A − NP and B − NP are completely repulsive, *i.e.*, only the r^{-12} term in $u_{ij}(r)$ above is considered. The full potential was employed for the NP − NP interactions only. To prevent the melting of the nanopump structure we employed a strong interaction between the NP particles, $\varepsilon_{\rm NP-NP} = 10\varepsilon_{\rm AA}$. All the interaction were truncated at 3.5 $\sigma_{\rm A}$. For the interaction parameters, we have used the values for Argon [27]: $\sigma_{\rm A} = 0.3405$ nm and $\varepsilon_{\rm AA}/k_B = 119.8$ K.

The system was constructed by solvating the nanopump in an equimolar mixture containing particles A and B in a fully periodic cell. The initial density and temperature were 6 particles/nm^3 and 250 K respectively. The nanopump was periodic in the x, y plane, while z defined the direction normal to the nanopump. A typical nanopump consisted of 4608 atoms, with surface area of 36.8 nm^2 and a thickness of 4.0 nm, solvated in 3600 fluid particles.

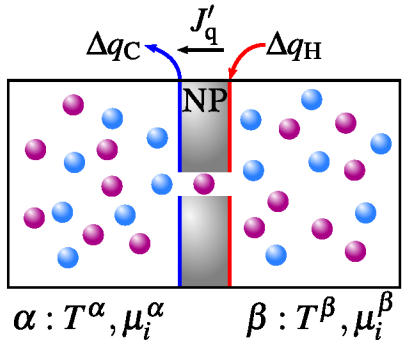

Fig. 1 Thermal nanopump model employed in this work. The two reservoirs, α and β are maintained at temperatures $T^{\alpha} = T_{\rm C}$ and $T^{\beta} = T_{\rm H}$ by adding ($\Delta q_{\rm H}$) and withdrawing energy ($\Delta q_{\rm C}$) at regular time intervals. $J'_{\rm q}$ represents the resulting heat flux across the nanopump, NP (color: gray). The two diffusing species are represented by spheres and colored blue and magenta. The chemical potential of specie $i = {\rm A, B}$ in compartment $x = \alpha, \beta$ is μ_i^x and in this system, a difference in chemical potential is established across the nanopump by thermodiffusion.

Following energy minimization and equilibration cycles a pore was sculpted in the nanopump by removing atoms within a predefined radius (*e.g.* 1.1 nm for NP1) of the axis passing through the centre of mass in the x, y plane. The system was replicated along the spatial z-direction, so that two compartments were generated. In Figure 2-right we show the structures we have considered in this work. After generating the

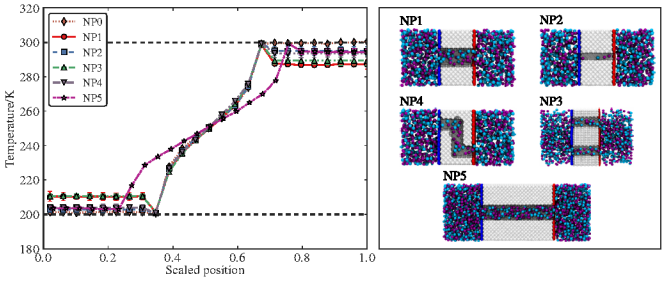

Fig. 2 The different nanopumps investigated in this work (right) and the steady temperature profile attained after approximately 1 ns (left). In NP0 only heat transfer is possible (this pore is included as a reference and the structure is not shown in the right figure), whereas NP1–5 allow heat and mass transfer. NP5 is 2.6 times longer than NP1–4 which are 4.0 nm long. The radius of the pore is 1.1 nm in NP1 and NP5, 0.78 nm in NP3 and NP4 and 0.47 nm in NP2. The temperature profiles are shown as function of the position in the box, scaled with the box-length.

structure we performed molecular dynamics simulations using the GROMACS [28] and LAMMPS [29,30] packages. Firstly an NVT simulation lasting between 6 and 25 ns (the longer simulation time were used for the narrower pores) was performed to equilibrate the fluid inside the nanopump. A configuration with a molar fraction 0.5 for each compartment was selected as the starting point for the non-equilibrium simulations.

Our model corresponds to an experimental situation where two reservoirs separated by the nanopump are maintained at constant temperatures, $T^{\alpha} = T_{\mathrm{C}}$ and $T^{\beta} = T_{\mathrm{H}}$. We imposed the thermal gradient across the nanopump by coupling two atomic layers in the solid structure (see Figure 1 and Figure 2) to heat baths using a suitable thermostat [31], and at temperatures 300 and 200 K. The system was propagated in time using the leapfrog integration scheme, with a time-step of 0.5 fs. The resulting heat flux, J_{q}, was obtained from the energy added/subtracted to/from the hot/cold thermostats $J_{\mathrm{q}} \equiv J_{\mathrm{U}} = \frac{\pm \Delta K}{\delta t A}$, where J_{U} is the internal energy flux (in the z-direction), ΔK is the average amount of kinetic energy added (+)/removed (−), over the course of a simulation, δt is the simulation time step and A the simulation box cross sectional area. The measurable heat flux is obtained from the total heat flux as $J'_{\mathrm{q}} = J_{\mathrm{q}} - J_{\mathrm{A}} H_{\mathrm{A}} + J_{\mathrm{B}} H_{\mathrm{B}}$, where H_i is the partial molar enthalpy of component i and J_i is the mass flux. The partial molar enthalpies were calculated in separate simulations as a function of the pressure and temperature. In all cases, the contribution from these terms were negligible ($\sim 1\%$ of the heat flux) so that $J'_{\mathrm{q}} \approx J_{\mathrm{q}}$.

This provides the desired conditions, namely, the thermal gradient is confined to the nanopump structure while the fluid reservoirs are maintained at constant temperature (see Figure 2-left and Figure 3-left). Hence the heat flux is zero in the bulk phases and reaches a constant value inside the nanopump structure (see Figure 3-right). The time scale needed to set the target temperature gradient, starting from a homogeneous temperature, $T = (T^{\alpha} + T^{\beta})/2$ in the whole system is less than 1 ns in all cases.

The temperature gradients employed in our study, $\nabla T \sim 10^{10}$ K/m, are routinely used in non-equilibrium computer simulations. It has been shown that the response of the system remains linear for these large thermal gradients [32,33]. This is consistent with the dimensionless relation, $\nabla T a \bar{T}^{-1} \ll 1$, which measures the relative importance of the thermal gradient to the thermal energy in terms of a characteristic length scale, a (the atomic diameter in this work) and $\bar{T}$ the average temperature of the system. We note that experiments are rapidly approaching the simulated thermal gradients. Indeed, very large thermal gradients, $\sim 10^9$ K/m have already been achieved in nanotube experiments [16].

We have investigated different pores to understand the impact of the pore geometry and structural parameters on the mass and heat transport (see Figure 2 and Table 1). In addition to cylindrical pore structures of different types (NP1–5) that enable heat and mass transport, we have considered as a reference a "blocked pump" (NP0), where heat can be transported but mass transport is not possible. The thermal conductivities (λ) for the nanopumps were calculated in separate simulations, in absence of fluid particles, as $\lambda = -J_{\mathrm{U}}/\nabla T$, where $\nabla T = (T_H - T_C)/\Delta z$, Δz being the thickness of the nanopumps.

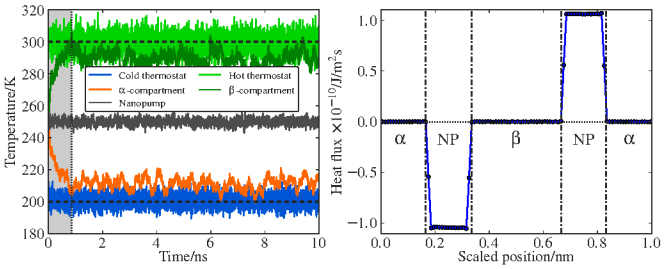

Fig. 3 Temperature evolution in NP1 (left) and the heat flux profile (right) in the direction normal to the nanopump across the simulation box. The temperature evolution is obtained by averaging over molecules residing in the different compartments and the two dashed lines indicate the set temperatures for the thermostatted hot and cold layers. The shaded area and the vertical dotted line in the left figure indicates the time needed to reach the stationary temperatures. The heat flux profile is averaged over times > 0.9 ns (the approximate time it takes to establish stationary temperatures in the two reservoirs). Here, the vertical dash-dotted lines show the different compartments, from left to right: α, NP (the nanopump) and β. Due to the computational setup the system is symmetric with respect to the midpoint along the direction of the temperature gradient. The heat flux is directed from the β-side of the nanopump towards the α-side of the nanopump.

Table 1 The radius and thermal conductivity (λ) of the nanopumps considered. The thickness of NP0–NP4 is 4.0 nm, while the thickness of NP5 is 10.4 nm

Nanopump	Radius/nm	λ/(W/K m)
NP0	–	0.46 ± 0.02
NP1	1.1	0.38 ± 0.02
NP2	0.47	0.42 ± 0.02
NP3	0.78	0.37 ± 0.02
NP4	0.78	0.37 ± 0.02
NP5	1.1	0.71 ± 0.02

To understand the impact of the nanopore thermal conductivity on the separation process we introduced vacancies of different types in two nanopores, NP1 and NP5. Advancing the discussion below, we find that these vacancies act as scatter centers for heat transport, reducing the thermal conductivity of the nanopump and increasing its thermodynamic efficiency.

We illustrate in Figures 3 and 4 the operation of the nanopump by evaluating the response functions, heat and mass

fluxes for NP1. In the initial state the two reservoirs have the same composition and temperature. Upon switching on the thermostats, the reservoirs reach the stationary cold and hot temperatures in about 1 ns. The temperature difference between the reservoirs drives the mass transport, but the timescale required to reach the stationary composition is longer than the time scale needed to achieve the stationary thermal transport (see Figures 4-left and 5).

We find that the final average composition in the reservoirs agrees well with a theoretical estimate based on kinetic theory[5]. In the steady state, the ratio of the temperature and concentration gradient is given by the Soret coefficient, s_T. For elastic spheres interacting through a repulsive r^{-12} potential, like the one employed in our work, the Soret coefficient can be expressed as an expansion in ascending powers of $(m_A - m_B)/(m_A + m_B)$. To the first order in this expansion[5], $s_T \approx \frac{0.504(m_A - m_B)}{T(m_A + m_B)}$, and a typical value of the Soret coefficient (for a temperature of order 10^2 K) is $s_T \sim 10^{-3}$ K^{-1}. This Soret coefficient is of the order expected for binary mixtures interacting through Lennard-Jones potentials (see *e.g.*[4,34]). Thus, the predicted separation is,

$$\Delta x_B = -x_B(1-x_B)s_T \Delta T \approx 0.041, \qquad (1)$$

such that $x_B^\beta = 0.5 + \Delta x_B/2 = 0.52$ ($x_B^\alpha \approx 0.48$) in the steady state. This is in good agreement with the final separation reached by the thermal nanopumps (see Figure 5), showing that the simple theory reviewed in reference[5] captures the separation in our fluid mixtures.

We note that recent investigations of simple fluids indicate that confinement has a small impact on the thermal diffusion factor[35].

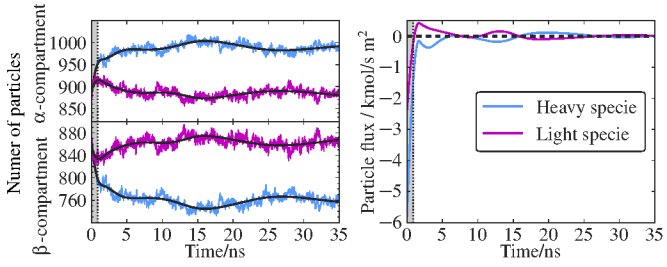

Fig. 4 (Left) The number of particles of the two species (blue: heavy specie (A), magenta: light specie (B)) in the two compartments as a function of time for NP1. (Right) The corresponding mass flux. The shaded area (color gray) shows indicated the time needed to reach the stationary temperatures in the two compartments.

3 Separation process and energy dissipation

We have examined above the general operation of the thermal nanopump. Now we turn to two practical questions. How fast is the separation process? And how efficient is it? To answer the first question we need to define a criterion to decide when the target concentration has been reached. To answer the second question we use the simulated fluxes and the corresponding thermodynamic forces to quantify the efficiency using non-equilibrium thermodynamic theory.

In order to estimate the time needed to reach stationary concentrations, we model the exchange of particles between the reservoirs as a first order rate process,

$$\mathrm{A}(\alpha) \underset{k_\alpha}{\overset{k_\beta}{\rightleftharpoons}} \mathrm{A}(\beta), \qquad (2)$$

where k_x is the kinetic constant associated with movement of particles into the x-compartment. In the steady-state, the concentration ratio of A in the two compartments ($C_A^{\alpha/\beta}$) is given by the rate constants, $k_\alpha/k_\beta = C_A^\alpha/C_A^\beta$, which fulfill $k_\alpha/k_\beta = 1$ at equilibrium conditions. However, away from equilibrium, *i.e.*, when the temperature gradient is present, $C_A^\alpha/C_A^\beta > 1$ and $k_\alpha > k_\beta$.

The time evolution of the mole fraction, obtained from this kinetic description is,

$$x_A^\alpha(t) - x_{A,f}^\alpha = \left(x_{A,0}^\alpha - x_{A,f}^\alpha\right) \mathrm{e}^{-(t-t_0)/\tau}, \qquad (3)$$

where $x_{A,f}^\alpha$ is the (final) mole fraction, obtained in the limit $t \to \infty$ and $x_{A,0}^\alpha = x_A^\alpha(t_0) = 0.5$ is the initial value. The time constant, $\tau = (k_\alpha + k_\beta)^{-1}$, quantifies the characteristic time of the separation process and we will later use this value to calculate the thermodynamic efficiency of the pump. In Figure 5 we show the molar fraction of the heavy component (A) as a function of time for nanopumps NP1–5 together with the kinetic theory estimated from Eq. (3). The good agreement between simulations and the theoretical model verifies the first order kinetics of the mass separation process investigated here.

The energy dissipated during the transport process can be quantified by calculating the entropy production of the system. In the system we consider, the temperature and concentration in the reservoirs are uniform over length-scales comparable to the thickness of the nanopore (see Figure 2-left). This effectively means that we only need to consider the entropy production of the surface, σ, given by[36],

$$\sigma = J_q' \left(\frac{1}{T^\beta} - \frac{1}{T^\alpha}\right) + \sum_{j=\{A,B\}} J_j \frac{\Delta_{\beta,\alpha}\mu_j(T^\beta)}{T^\beta}, \qquad (4)$$

we note that σ is given per unit area of the surface, which is defined here as the full cross sectional area of the box. We

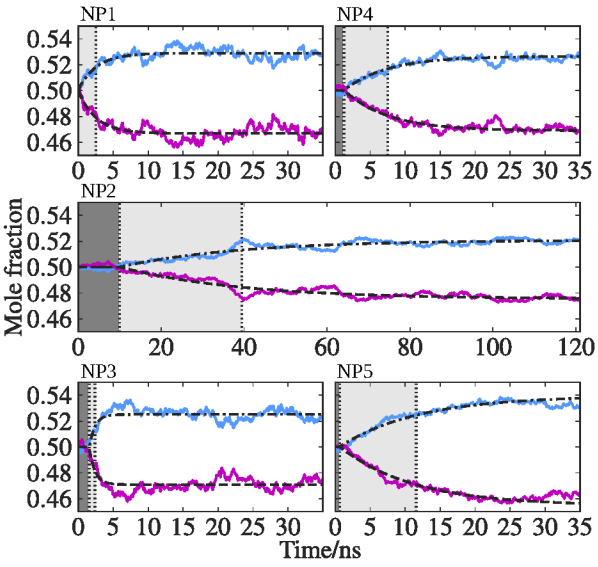

Fig. 5 Molar fraction of the heavy specie (A) in the cold (color blue) and hot (color magenta) compartments as a function of time for nanopumps NP1–5 (from top to bottom). The separation in NP2 is much slower that the other pores and for this pore, we show the time evolution up to 120 ns. For all pores, the mole fraction was calculated as the average over three independent simulations, starting from different initial states, with equal average temperature (250 K) and equal mole fractions (1/2 in both compartments). The black lines (dashed and dash-dotted) show the exponential fit, using Eq. (3), to the time evolution of the mole fractions in the two compartments. The shaded areas (dark and light gray) separated with the vertical dotted lines show the two characteristic times (t_0 and τ) obtained from the fit of Eq. (3): the dark gray area represents the time t_0 while the lighter gray area represents τ. For quantifying the efficiency, we will later use the total shaded area.

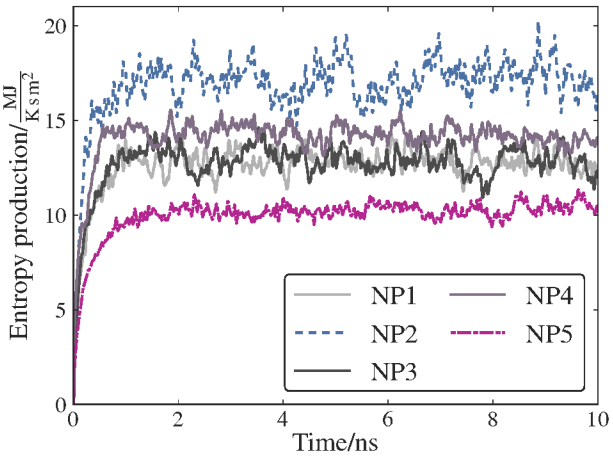

Fig. 6 The entropy production for the different nanopumps considered in this work, NP1–5, obtained from Eq. (4) as described in the text. The entropy production is largest for NP2 (dashed line) while NP5 (dash-dotted line) gives a smaller entropy production.

obtain the measurable heat flux through the surface, J'_q and the mass flux J_j as previously described. For the difference in chemical potential of component j in the two compartments ($\Delta_{\beta,\alpha}\mu_j(T^\beta) = \mu_j^\beta(T^\beta) - \mu_j^\alpha(T^\beta)$) we have approximated the solution as an ideal solution. This is justified since the fluid interactions A-A, B-B and A-B are identical and purely repulsive in our system.

We show in Figure 6 the time dependence of the entropy production. Upon a short transient period σ reaches a stationary value where the nanopump dissipates energy at a constant rate. Interestingly the dissipation depends strongly on the nanopump structure. Since the heat flux is two orders of magnitude higher than the mass flux in these nanopumps, the heat transfer dominates the dissipation (see Eq. (4)), meaning that nanopumps with higher heat fluxes, dissipate more. For system subjected to identical temperature gradients (*e.g.* NP1–4), the heat flux is determined by the thermal conductivity, λ, and the dissipation must increase with the conductivity: worse conductors dissipate less. This is indeed the case as can be seen by comparing NP2 with NP1/3/4 (See Table 1 and Figure 6). The dissipation of pore NP5 is lower, despite having a larger thermal conductivity than other pores. We note that this pore is thicker, hence, the resulting temperature gradient across the pore is smaller, resulting in a reduction of the heat flux and the dissipation.

The investigation of pores containing defects provides a route to examine the impact of the pore thermal conductivity on the dissipation rate. We introduce defects in the nanopores, NP1 and NP5, by randomly removing 12% and 6% of the atoms to get two new structures NP1* and NP5*. For NP1 we also consider a second structure NP1′ obtained by removing the same amount of atoms as in NP1*, *i.e.*, same volume fraction of defects, but using a different spatial distribution for the defects, so that they now form spherical empty regions in the nanopump (see Figure 7). To construct the NP1′ structure, we defined four points in the middle of the nanopump and 2.7 nm away from the nanopump surface. All the atoms within 1 nm of the center of these points were eliminated.

The thermal conductivities of the modified structures are shown in Table 2 and entropy production of the modified nanopumps are shown in Figure 7. The entropy production follows the trends observed in the thermal conductivity. For pores of the same thickness, those with lower thermal conductivity result in lower energy dissipation rates (entropy production) when considering identical temperature gradients.

Table 2 The radius and thermal conductivity (λ) of the modified nanopumps. The thickness of the modified pores are equal to the unmodified structure (4.0 nm for NP1* and NP1′ and 10.4 nm for NP5*). The relative thermal conductivity (λ_0/λ) is calculated with respect to the unmodified structure (λ_0): NP1 for pores NP1* and NP1′, and NP5 for NP5*.

Nanopump	Radius/nm	λ/(W/K m)	λ_0/λ
NP1*	1.1	0.22 ± 0.02	1.7 ± 0.2
NP1′	1.1	0.27 ± 0.02	1.41 ± 0.13
NP5*	1.1	0.35 ± 0.02	2.03 ± 0.13

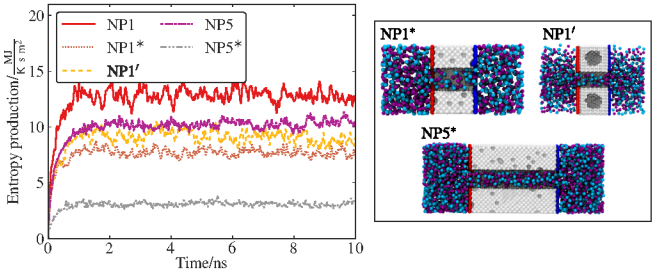

Fig. 7 Entropy production (left) and structure (right) of the modified nanopumps NP1*, NP1′ and NP5*.

4 How efficient are the thermal nanopumps?

The *thermodynamic efficiency* of the nanopumps can be quantified by observing the operation of the pump over a period of time, Δt. During this time, the pump moves particles between the two reservoirs and performs a certain amount of work. The efficiency is the ideal or minimum amount of work (ΔW_{id}) associated with the operation of the pump, divided by the actual work done, which is given by the sum of the ideal work and the lost work (ΔW_{lost}) due to the dissipation. The efficiency, η, is then,

$$\eta = \frac{\Delta W_{\mathrm{id}}}{\Delta W_{\mathrm{lost}} + \Delta W_{\mathrm{id}}}, \tag{5}$$

where the lost work can be obtained from the dissipation rate,

$$\Delta W_{\mathrm{lost}} = \bar{T} A \int_{t}^{t+\Delta t} \sigma(t')\,\mathrm{d}t'. \tag{6}$$

The ideal work, ΔW_{id}, is the work required to separate the mixture and it is defined by the free energy required to move particles from one reservoir to the other, taking into account the concomitant change in temperature and composition,

$$\Delta W_{\mathrm{id}} = \frac{1}{A} \sum_{j=\{A,B\}} \Delta \left(n_j^{\alpha} \mu_j^{\alpha} + n_j^{\beta} \mu_j^{\beta} \right). \tag{7}$$

The chemical potential is here given by,

$$\mu_j^{\beta} = \mu_j^{*} + RT^{\beta} \ln x_j^{\beta},$$

where μ_j^{*} is the chemical potential of the pure system and we continue our ideal approximation for the mixture. We obtain the chemical potential of the pure component by performing additional equilibrium simulations, using the test particle insertion method[37] for several conditions. We then interpolate the calculated chemical potentials in order to obtain $\mu^{*}(\rho, T)$ as a function of the number density, ρ and temperature. For the interpolation, we have considered a bivariate spline of the 4-th degree in the two variables $\exp(-\hat{\rho})$ and $(T \times \hat{\rho})$, where $\hat{\rho}$ is the unitless number density. The results from this interpolation is shown in Figure 8.

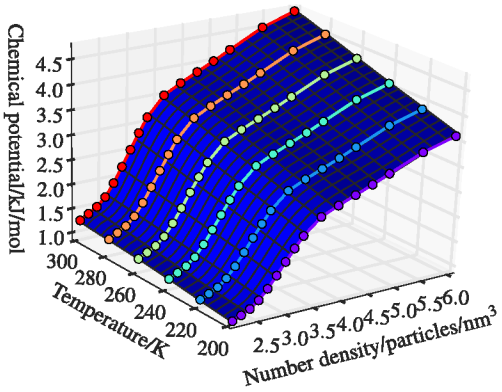

Fig. 8 The chemical potential as a function of temperature and number density as calculated by the test particle insertion method (circles). The blue surface is an interpolation (see Methods) through the simulated data.

Equation (5) shows that the efficiency of the process depends on the amount of energy dissipation, $\Delta W_{\mathrm{lost}} \sim \sigma$, but also on the time scale associated to this dissipation, Δt. As $t \to \infty$, the ideal work reaches a stationary value since there are no *net* changes of compositions or temperatures in the stationary state. The lost work, however, continues to grow with increasing t. This means that the efficiency will approach 0 as $t \to \infty$. In order to calculate the efficiency of the different nanopumps using eqns. (5)– (7), we therefore use the characteristic time scale for separation, which can be estimated from eq. (3). Hence, we set $\Delta t = \tau + t_0$ which corresponds to the shaded area in Figure 5. We thus determine the efficiency of the separation process in terms of the characteristic time needed to reach the stationary concentration and the energy dissipated in reaching this state.

Our simulations show that the pore geometry has a significant impact on the characteristic timescale for separation, with the shorter pores, NP1 and NP3 resulting in a faster separation. Stationary concentrations are reached in a few ns. Adding tortuosity to the pore (maintaining the pore surface area), see NP4, a situation that is relevant in membrane structures used in filtration, increases the time scale needed to achieve separation. We have further considered a situation in which we use

nanopores of intermediate radius, NP3 (pore radius $\sim 2.3\sigma_A$), but whose combined surface area is the same as that of the single pore modeled in NP1 (pore radius $\sim 3.2\sigma_A$). Splitting the larger pore in two smaller ones decreases the separation time. However we expect this enhancement will be limited by steric effects, which will become relevant in very narrow pores, hence limiting the diffusion process. Indeed, the examination of a very narrow pore, NP2 (pore radius $\sim 1.38\sigma_A \sim$ 0.5 nm), which results in very slow diffusion (see Figure 5), shows the characteristic separation time increases by one order of magnitude! We note that the characteristic pore sizes considered here are similar to those that can be achieved with nanotubes, hence our results should be relevant to technologies based on those nanomaterials.

The time scale needed to achieve the stationary concentration has a large impact on the thermodynamic efficiency. We examine in Table 3 this efficiency for a range of thermal nanopumps investigated in this work. The efficiency for nanopumps NP1-5 is very low in general reaching maximum, 0.15%, and minimum, 0.007%, values for pores NP3 and NP2 respectively. Our lower efficiency is similar to the one reported in studies of model nanomotors powered with chemical reactions, ($\sim 0.02\%$[26]). The variation we observe in the efficiencies can be rationalized by considering the timescales needed to reach the stationary concentrations as well as the amount of energy dissipated in reaching this stationary state. As shown in eqns. (5) and (6), these two variables are interlinked, namely, the longer the time scale of the process the large the lost work and the lower the efficiency. Pores involving longer time scales for mass separation are less efficient. This effect is particularly well illustrated with the results obtained for pore NP2. This is a very narrow pore and mass flux is very slow. Hence, significantly more energy is wasted to achieve the stationary composition. Moreover NP2 features a larger thermal conductivity than nanopumps of similar thickness, which results in a larger heat flux and larger dissipation (see Figure 6). All these factors contribute to the lower efficiency observed in the NP2 nanopump. Our results illustrate an important notion. For pores that are close to the typical dimensions of nanotubes we find that the efficiency can be increased significantly by tuning the nanopore radius. Indeed increasing the pore radius by a factor of ~ 2 (from NP2 to NP1) results in a significant gain in efficiency, ≈ 20 times. Our results also show that increasing the pore density can in some cases outweigh the enhancement in efficiency associated to the increase in the pore radius (cf. NP1 and NP3 in Table 3). We have shown so far that the efficiency of the pumping process can be modified by modifying the pore structure. Even for the most efficient structures the efficiency of the nanopumps is very low, $< 0.2\%$. How can we enhance the efficiency to more acceptable values, *e.g.* closer to 1%? It is clear from the discussion above that the efficiency is determined by both mass transport and energy dissipation. The former is determined to a large extent by the pore geometry, while the heat flux represents the dominant contribution to the latter. The heat flux and therefore the entropy production (energy dissipated) can be reduced by decreasing the thermal conductivity of the nanopump. Addition of scattering centers, *i.e.*, defects in the crystal structure, should reduce the thermal conductivity by modifying the heat carrier's mean free path, with the advantage that the nanopore structure is not modified. We find that the introduction of these defects is fairly effective and reduces significantly the thermal conductivity of the nanopump with respect to the original structure (cf. NP1, NP1* and NP1$'$ in Table 3). The decrease in the thermal conductivity has also an impact on the entropy production, which is smaller for the nanopumps containing nanoscale defects. These pores are much more efficient, reaching more acceptable values, of the order of 0.5% (see Figure 9).

Table 3 Characteristic time scale (τ) for the nano pumps, obtained from the kinetic model and the efficiency calculated using the non-equilibrium theory.

Nano-pore	Time constant (τ/ns)	Characteristic time $(\tau + t_0)$/ns	Efficiency ($\eta \times 100$)
NP1	2.58 ± 0.04	2.58 ± 0.04	0.14 ± 0.01
NP1*	0.73 ± 0.02	1.38 ± 0.02	0.52 ± 0.04
NP1$'$	0.80 ± 0.02	1.44 ± 0.02	0.49 ± 0.02
NP2	29.4 ± 0.2	39.4 ± 0.2	0.007 ± 0.002
NP3	0.83 ± 0.02	2.40 ± 0.02	0.15 ± 0.02
NP4	6.27 ± 0.04	7.50 ± 0.04	0.050 ± 0.007
NP5	10.93 ± 0.06	11.57 ± 0.06	0.070 ± 0.010
NP5*	8.94 ± 0.08	10.57 ± 0.08	0.24 ± 0.08

We have explored further this idea by considering longer pores, NP5 and NP5*. As expected increasing the pore length leads to longer separation times (see Table 3) and high thermal conductivities (see Table 1 and 2), with a consequently low thermodynamic efficiency, 0.07%. We find that adding nanoscale defects decreases the thermal conductivity significantly (see Table 2), and trebles the efficiency, $\sim 0.2\%$ (see Figure 9).

5 Summary and Conclusions

We have investigated mass separation in binary mixtures using nanopores with different geometries and thermal properties. The driving force for the mass separation is furnished by thermal gradients that drive the Soret-Ludwig effect, such that heavy and light particles concentrate in cold and hot regions respectively. The combination of classical non-equilibrium molecular dynamics simulations and non-equilibrium thermodynamics theory provides a powerful approach to quantify the

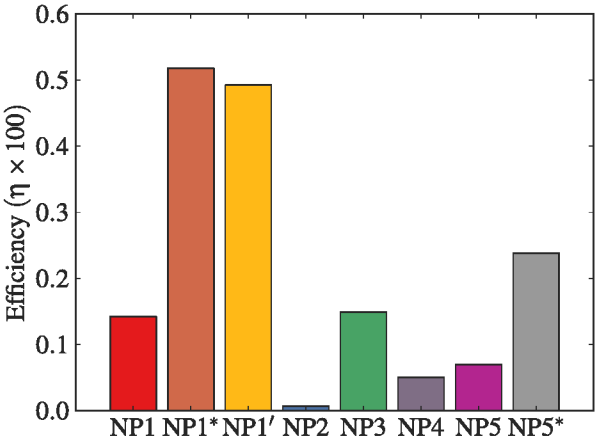

Fig. 9 Efficiency of the different nanopumps. As discussed in the text, the efficiency increases significantly by modifying the thermal conductivity, as can be seen by comparing the efficiency of NP1 with NP1*/NP1′ and NP5 with NP5*

thermodynamic efficiency of the transport process. We have shown that the thermodynamic efficiency is determined by a complex interplay of time and energy scales, which can be accessed using our computational approach. We have developed a general kinetic model and a non-equilibrium theory approach that in combination with the simulation data provides a route to quantify the efficiency.

We have shown that the pore radius has a large impact on the time scale needed to reach the stationary compositions. Doubling the pore radius reduces this time scale by a factor of 15 (from 40 ns for a 0.47 nm radius to 2.5 ns for 1.1 nm radius). This enhancement in the diffusion results in an equivalent increase, ~ 15 times, in the thermodynamic efficiency. We have also shown that the enhancement in the efficiency can be increased even more at the cost of reducing the pore radius (down to 0.78 nm) by increasing the pore density. Our results show that the manipulation of pore radius and pore density is a powerful approach to enhance the efficiency of the separation process.

Our results indicate that the efficiency of thermal nanopumps will in general be very low. Typical efficiencies lie between 0.01% and 0.1%, which are very far from the Carnot efficiency (30%) that would be obtained for a thermal machine operating with temperature gradients similar to those investigated in this work. This large difference exposes the limitations of macroscopic thermodynamic approaches to quantify the efficiency of nanoscale devices.

The lowest thermodynamic efficiencies obtained in this work are similar to those reported in model nanomotors fuelled with chemical reactions. Although these low efficiencies are expected to represent a relatively minor problem in devices that are intended to use "waste heat", we have shown that it is possible to increase the efficiency significantly, $> 0.5\%$ by manipulating the material thermal properties. The heat flux across the nanopore represents the main contribution to the energy dissipated by the nanopump. Hence we targeted the reduction of the heat flux as a main objective. We have shown that this reduction can be achieved by reducing the thermal conductivity of the nanopump, which from a practical point of view can be modified by adding nanoscale defects that act as scattering centers for the heat carriers. A nanopump with such defects features significantly lower thermal conductivities and a large enhancement in the thermodynamic efficiency. We have found an increases of the order of $3-4$ times in the efficiency, bringing the latter to values of the order of 0.5%. Hence, nanostructures featuring large thermal resistance should be more efficient.

Overall we have shown a model for a thermophoretic separation device, and showed how the efficiency can be significantly improved by modifying the geometry and thermal transport properties of the device. Our work highlights the limitations of macroscopic approaches that focus on the properties of the bulk phases and neglect the interfacial properties of the nanopore. Fine tuning of the nanopore properties should lead to significant gains in device operation.

Our approach can be extended to investigate a whole range of nanostructures, fluid mixtures, and driving forces, opening new opportunities to quantify the thermodynamic efficiency of a wide range of nanoscale devices. The pores investigated in this work have diameters similar to carbon nanotubes (CNT) and they are in the lower end of silicon nitride (SiN) solid state pores. Our results should therefore be relevant to technological applications that use CNT or SiN structures, such as nanofluidic, separation and sensing devices.

Acknowledgements

Financial support for this work was provided by the EPSRC (EP/J003859/1). F. Bresme thank the EPSRC for the award of a Leadership Fellowship and A. Lervik thank JETC for the award of the Prigogine Prize. We acknowledge the Imperial College High Performance Computing Service for providing computational resources.

References

1 E. Pop, *Nano Research*, 2010, **3**, 147–169.
2 S. de Groot and P. Mazur, *Non-Equilibrium Thermodynamics*, Dover, New York, 1984.
3 F. Bresme, A. Lervik, D. Bedeaux and S. Kjelstrup, *Phys. Rev. Lett.*, 2011, **101**, 020602.
4 F. Römer, F. Bresme, J. Muscatello and J. Rubi, *Phys. Rev. Lett.*, 2012, **108**, 105901.
5 R. C. Jones and W. H. Furry, *Rev. Mod. Phys.*, 1946, **18**, 151–224.
6 D. Braun and A. Libchaber, 2002, **89**, 188103.

7 S. Wiegand, *J. Phys.: Condens. Matter*, 2004, **16**, R357–R379.
8 C. Wienken, P. Baaske, U. Rothbauer, D. Braun and S. Duhr, *Nature Communications*, 2010, **1**, 100.
9 J. E. Reiner, J. W. F. Robertson, D. L. Burden, L. K. Burden, A. Balijepalli and J. J. Kasianowicz, 2013, **135**, 3087–3094.
10 C. Dekker, *Nature Nanotechnology*, 2007, **2**, 212–215.
11 D. Branton, D. W. Deamer, A. Marziali, H. Bayley, S. A. Benner, T. Butler, M. Di Ventra, S. Garaj, A. Hibbs, X. Huang, S. B. Jovanovich, P. S. Krstic, S. Lindsay, X. S. Ling, C. H. Mastrangelo, A. Meller, J. S. Oliver, Y. V. Pershin, J. M. Ramsey, R. Riehn, G. V. Soni, V. Tabard-Cossa, M. Wanunu, M. Wiggin and J. A. Schloss, *Nature Biotechnology*, 2008, **26**, 1146–1153.
12 N. Sa, W.-J. Lan, W. Shi and L. Baker, *ACS Nano*, 2013, **7**, 11272–11282.
13 Y. He, M. Tsutsui, R. Scheicher, F. Bai, M. Taniguichi and T. Kawai, *ACS Nano*, 2013, **7**, 538–546.
14 M. Yang and M. Ripoll, *Soft Matter*, 2014, **10**, 1006–1011.
15 H. Jiang, H. Wada, N. Yoshinaga and M. Sano, *PRL*, 2009, **102**, 208301.
16 A. Barreiro, R. Rurali, E. Hernandez, J. Moser, T. Pichler, L. Forro and A. Bachtold, 2008, **320**, 775–778.
17 R. Qiaio, J. Georgiadis and N. Aluru, *Nano Letters*, 2006, **6**, 995–999.
18 C. Sathe, X. Zou, J.-P. Leburton and K. Schulten, *ACS Nano*, 2011, **5**, 8843–8851.
19 S. Adiga, *Nano Lett.*, 2005, **5**, 2509–2514.
20 P. Gaspard and D. Andrieux, *J. Stat. Mec.*, 2011, **3**, P03024.
21 K. Kinosita, R. Yasuda, H. Noji and K. Adachi, *Philos. Trans. R. Soc. Lond. B Biol. Sci.*, 2000, **355**, 473–489.
22 C. Bustamante, J. Liphardt and F. Ritort, *Phys. Today*, 2005, **58**, 43–48.
23 K. Kawaguchi, *FEBS Lett.*, 2008, **582**, 3719–3722.
24 J. V. Møller, C. Olesen, A.-M. L. Winther and P. Nissen, *Q. Rev. Biophys.*, 2010, **43**, 501–566.
25 A. Lervik, F. Bresme, S. Kjelstrup and J. Rubí, *Biophys. J.*, 2012, **103**, 1218–1226.
26 Y. Shi, L. Huang and D. W. Brenner, *The Journal of Chemical Physics*, 2009, **131**, 014705.
27 L. Rowley, D. Nicholson and N. Parsonage, *Journal of Computational Physics*, 1975, **17**, 401–414.
28 B. Hess, C. Kutzner, D. van der Spoel and E. Lindahl, *Journal of Chemical Theory and Computation*, 2008, **4**, 435–447.
29 S. Plimpton, *Journal of Computational Physics*, 1995, **117**, 1–19.
30 `http://lammps.sandia.gov/`.
31 G. Bussi, T. Zykova-Timan and M. Parrinello, *The Journal of Chemical Physics*, 2009, **130**, 074101.
32 F. Römer, A. Lervik and F. Bresme, *J. Chem. Phys.*, 2012, **137**, 074503.
33 F. Bresme and J. Armstrong, *JCP*, 2014, **140**, 16102.
34 P. Artola and B. Rousseau, *Mol. Phys.*, 2013, **111**, 3394–3402.
35 R. Hannaoui, G. Galliero, H. Hoang and C. Boned, *J. Chem. Phys.*, 2013, **139**, 114704.
36 S. Kjelstrup and D. Bedeaux, *Non-Equilibrium Thermodynamics of Heterogeneous Systems*, World Scientific, Singapore, 2008.
37 B. Widom, *J. Chem. Phys.*, 1963, **39**, 2808–2812.

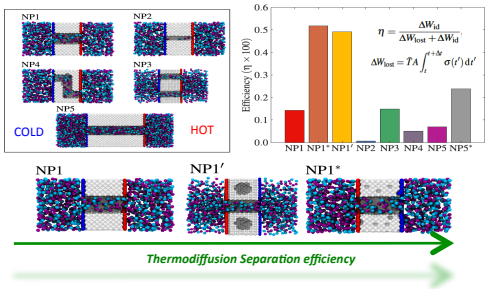

Caption Graphical Abstract:
Nanoscale structural defects significantly enhance the efficiency of particle separation using thermally driven nanopumps